Progress In Electromagnetics Research M, Vol. 100, 197–211, 2021

Investigation of Ionospheric Vertical Delay at S1 and L5 Frequencies, Based on Thick-Shell Model Using NavIC System, for Mid Latitude Region of India

Sharat C. Bhardwaj[1, *], Anurag Vidyarthi[1], Bhajan S. Jassal[1], and Ashish K. Shukla[2]

Abstract—To meet the growing requirements of Standard Positioning Services (SPS) and Precision Services (PS), more and more GNSS systems operating at conventional GPS frequencies and higher frequency bands are launched. The Indian NavIC system is one of such systems transmitting navigational signals at S1 (2492.028 MHz) and L5 (1176.45 MHz) frequencies. For GPS at L-band frequencies, comprehensive research work has been conducted to analyze the ionospheric delay to estimate precise user position, although very little research work is available in the public domain at the navigational S-band level. The NavIC program provides opportunities to explore the ionospheric delay effect on S-band navigational signals. The precise position determination demands accurate estimation of the vertical ionospheric delay which is generally obtained using Vertical Electron Content (VTEC) of the ionosphere. The VTEC can be obtained by multiplying a mapping function to the Slant Total Electron Content (STEC). Conventionally a thin shell (also known as a single shell) model is used to map STEC to VTEC, but it introduces error at low elevation angles. This error is significant for the NavIC receivers, located in the northern part of India, as they observe elevation angles below 50° for most of the time, and thus there is a need to investigate the suitability of the mapping function model for the NavIC system. As the ionospheric shell height modifies the mapping function and results in a change in VTEC, the height and thickness of the thick shell have been investigated based on the ionospheric data taken from IRI 2016 and were estimated as 300 km and 250 km, respectively. In the present work, the thick shell model has been compared to thin shell model mapping functions to improve the accuracy of VTEC estimation at the low elevation. The reduction in vertical delay using the thick shell mapping function at low elevation indicates its suitability for the locations like Dehradun, India, which lies in the mid-latitude region. Furthermore, the temporal variability of vertical delay at S and L band frequencies has also been investigated to understand the diurnal and seasonal characteristics of ionospheric vertical delay over a period of 12 months to cover all the seasons during the year 2017–18. The vertical delay at the S-band frequency was found to be less than that at the L-band frequency and is almost constant over a month. This finding will be beneficial for single-frequency users and could be used to develop the Grid Ionospheric Vertical Delay (GIVD) map for the NavIC system to enhance positional accuracy.

1. INTRODUCTION

In recent years, there has been a tremendous increase in demand for trans-ionospheric communication systems used for the navigation of spaceborne vehicles (such as satellites and aircraft) and surface transportation systems. To meet these requirements, Global Navigation Satellite Systems (GNSS), like

Received 23 November 2020, Accepted 13 January 2021, Scheduled 28 January 2021
* Corresponding author: Sharat Chandra Bhardwaj (bhardwaj.sharat@gmail.com).
[1] Department of Electronics and Communication, Graphic Era (deemed to be) University, Dehradun, India. [2] Space Applications Center, Indian Space Research Organization, Ahmedabad, India.

GPS, Glonass, Galileo, BeiDou, and regional navigation satellite systems like NavIC (Navigation with Indian Constellation) and QZSS, have been launched by different countries. These airborne navigation systems are also used for satellite-based augmentation systems (SBAS) developed worldwide for airline navigation. The Indian Space Research Organization (ISRO) has been developing GPS Aided Geo Augmentation Navigation (GAGAN) system in collaboration with the Airports Authority of India intended to enhance the accuracy and integrity of user position estimates [1]. In some literature, it is predicted that more than 150 satellites and 400 signals will be present in space by 2030 for navigation only [2, 3]. Therefore, sharing the same frequency band for such a large number of signals in the L-band will create signal congestion and may deteriorate the performance of the systems. To avoid this radical situation for future navigation systems, new frequency bands have been introduced in addition to the GPS frequencies. The International Telecommunication Union (ITU) has allocated S-band, between 2483.5 MHz and 2500 MHz, for navigation services [4]. Therefore, it is the right time to explore the S-band signals along with L-band signals and their effect on positioning accuracy and timing performance of radio navigation services [5–7].

In the case of satellite-based navigation systems, the accuracy of estimated positional parameters gets affected by the errors introduced by the ionosphere, satellite-receiver geometry, troposphere, multipath, instrumental biases, etc. Among all, the ionosphere is the major source of error. The measurement of the line-of-sight distance between satellite and receiver gets affected by the ionospheric delay introduced due to the interaction between the electrons in the ionosphere and the electromagnetic radiations received from the satellite. The magnitude of the ionospheric delay depends on the carrier wave frequency and the Total Electron Content (TEC) along the slant or vertical path, as the case may be, between the satellite and receiver. The positive ions in the ionosphere are 2,000 to 60,000 times heavier than the electrons and so their range of movement, caused by the electric field of the radio waves, is smaller than that of electrons in the proportion of their weight. Hence, the effects of ions on the propagation of radio signals are ignored [8]. Furthermore, there is a second-order ionospheric delay present in the satellite range measurement due to the interaction among the electromagnetic radiations, electrons in the ionosphere, and the earth's magnetic field. In the present work, only the first-order vertical delay (or Vertical Delay) is investigated.

The various satellite-based navigation systems derive ionospheric delay error and confidence bound from the estimates of vertical ionospheric delay modeled on a grid at regularly spaced intervals of latitude and longitude ($5^\circ \times 5^\circ$) of the GIVD (Grid Ionospheric Vertical Delay) map. The vertical delay at each Ionospheric Grid Point (IGP) is calculated from a planar fit of delay measurements at neighboring points. The vertical delay at the user position is obtained by interpolation from the delay values at the neighboring grid points. The product of the interpolated value with the obliquity factor, also known as mapping function, provides an estimate of the slant ionospheric delay [9]. For the estimation of vertical/slant ionospheric delay, researchers have suggested various models [10, 11], such as a thin-shell ionospheric model [12], Klobuchar model [13], IGP-based model [14], Ionosphere-tomography model [15–17], two-shell [18], and multi-shell models [19]. Out of them, the thin-shell model, which is mathematically more straightforward, is the most popular and widely used for ionospheric delay estimation. In this model, the whole ionosphere is assumed as a 2D shell with infinitesimal thickness located at a particular altitude. Generally, this altitude is taken as the height of the maximum electron density of the ionosphere [20]. This assumption reduces a complex volumetric conversion problem of slant to vertical TEC into a simple planar form. The point where the line of sight of the satellite from the receiver intercepts the shell is defined as the ionospheric pierce point (IPP). However, this conversion of 3D ionosphere geometry into the 2D model affects the accuracy of vertical TEC (VTEC) estimated from slant TEC (STEC) as the mapping function for the thin shell model is solely dependent on the shell height [21]. Any change in the shell height modifies the mapping faction and the coordinates of IPP, which results into change in the latitude profile of VTEC [22]. The angle between the vertical and ray path at IPP decreases with an increase in ionospheric height and increases VTEC, determined from STEC, especially at lower elevation angles. Xiang and Gao [23] compared available mapping functions and found that the variation of shell height from 350 km to 450 km results into the change in mapping function up to 10% at a 10° masking angle which is the minimum acceptable elevation angle above the horizon that a GPS satellite has to be at to avoid blockage of line-of-sight.

An intensive study has been done to find the effective height of the thin-shell model. Lanyi and

Roth [24] proposed the height between 350 and 400 km. Hernàndez-Pajares et al. [25] derived the height ranging from 350 to 650 km using comprehensive GPS data. The study by Brunini et al. [26] shows the effect of single-shell height (between 300 and 550 km) on VTEC and Differential Instrumental biases (DIBs) estimation. In these works, it is concluded that fixed height does not achieve zero conversion error, and the error is also affected by solar activities and the latitude of the receiver. For the Indian equatorial and low latitude regions, Prasad et al. [27] suggested an IPP altitude of 350 km for the elevation angles above 50°. To overcome the problem of shell altitude variation with diurnal and seasonal changes, particularly in the Indian regions, a two or multi-shell model may be a better choice [28–30]. Shukla et al. [18] implemented a two-shell ionospheric model based on the planar fit model over the Indian low-latitude region. In this approach, vertical TEC values are estimated for the two shells separately and added for the final value. However, it requires computational process and number of coefficients for all IGP locations over a wide area. Ratnam et al. [29] and Maruyama et al. [31] proposed a multi-shell approach by using the Spherical Harmonic Function (SHF) estimation technique for VTEC modeling over the low-latitude Indian sub-continental region and near the magnetic equator using local receiver network, respectively. Although this SHF model represents the ionospheric behavior with fewer coefficients, it suffers from computational complexity at multiple IPP points for a single receiver. Also, it lacks realistic VTEC estimation for modeling applications over the Indian region, and there is also no discussion on the choice of shell altitude.

Minimal literature, based on the multi-shell approach, has been found to deal with the accuracy of ionospheric delay estimation at lower elevation angles [19]. However, this approach requires multiple IPP based coefficients estimation, and the study is limited to mid-latitude regions. Literature shows that significant work has been done on vertical delay for higher elevation angles, but not much work is reported for the low elevation angle at the low- or mid-latitude regions. The reason is that most of the studies on mapping function have been done for GPS, where the receiver mostly observes high elevation angles ($> 70°$). At higher elevation angle, inaccuracy in the conversion of STEC into VTEC due to mapping function is less; even for the elevation angles greater than 70° STEC can be considered as VTEC. On the other hand, when the elevation angle is low, the amount of error due to inaccurate mapping function is increased. A comparative study, done by Smith et al. [30], shows that the modeling of the ionosphere using a two-dimensional shell can introduce an error up to 50% at low elevation angle (30° or less). This finding is important for the NavIC receivers, located in the northern part of India [32], as they observe elevation angles below 50° for most of the time [33]. With this in view, it is felt that there is a need to investigate the mapping function modeling for NavIC system at low elevation angles.

NavIC is a regional navigation satellite system that has been launched to provide independently Standard Positioning Service (SPS) and Precision Service (PS) at S1 (2492.028 MHz) and L5 (1176.45 MHz) frequencies. The NavIC system consists of three geostationary and four geosynchronous satellites. The geostationary satellites are located at 32.5°E (PRN 6), 83°E (PRN 3), and 131.5°E (PRN 7) longitudes. The geosynchronous satellites are moving in independent 29° inclined orbits; two crossing the equator at 55°E (PRN 1, 2) and the other two at 111.75°E (PRN 4,5) longitude. It is designed to provide accurate position information service to users in India as well as the region extending up to 1500 km from its boundary [34].

In the present paper, a spherical thick shell model of ionosphere, with a homogeneous distribution of free electrons, has been considered for the estimation of VTEC and the ionospheric vertical delay, based on data collected in the year 2018 at S and L band frequencies in Dehradun using NavIC system. The modal considers the IPP at the height of the maximum electron density, i.e., F2 layer (hmF2). The height and thickness of the shell have been estimated using data from International Reference Ionosphere (IRI 2016) [35] for the year 2018. A comparison has been made between thick and thin shell model mapping functions to show the effect of low elevation angle on VTEC estimation from experimentally determined STEC. A seasonal analysis of vertical delay estimated using at S1 and L5 frequencies is carried out for the study of temporal variability. The following sections of this paper deal with the data collection, estimation of parameters for the thick shell ionospheric model, and estimation of vertical delay.

2. SPHERICAL THICK SHELL IONOSPHERIC MODEL

In thick shell model ionosphere is assumed to be concentrated with uniform electron density between two boundaries. The thickness of the shell, also called slab thickness, is taken as the ratio of vertical TEC to the maximum electron density. The geometry of the thick shell is shown in Fig. 1.

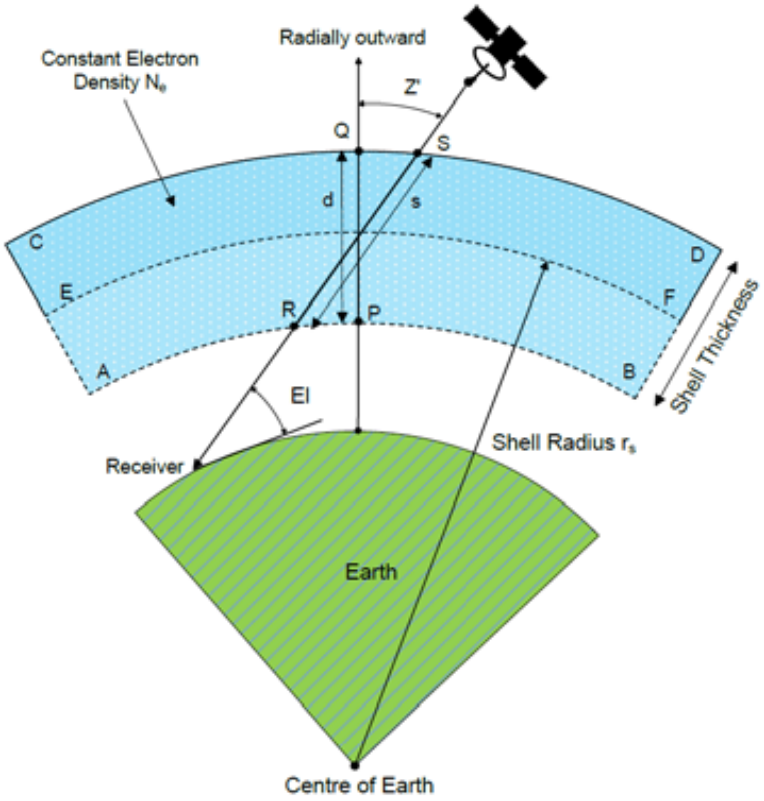

Figure 1. Geometry of spherical thick shell ionospheric model.

In Fig. 1, lines AB and CD show the lower and upper boundaries of the shell. The thickness of the shell (PQ) and the slant path line (RS) are denoted by d and s, respectively. The central line EF represents the shell height taken as the height of maximum electron density (hmF2). The point where the slant path line crosses the central line EF is considered as Ionospheric Pierce Point (IPP). The angle between PQ and RS at IPP is known as the zenith angle (Z').

The mapping function for the spherical thick shell is given as [21, 30]

$$M_s = \frac{1}{d}\left[\sqrt{\left(r_s + \frac{d}{2}\right)^2 - (r_s \sin Z')^2} - \sqrt{\left(r_s - \frac{d}{2}\right)^2 - (r_s \sin Z')^2}\right] \tag{1}$$

where r_s is the radius of curvature of the line EF, and d is the shell thickness.

In terms of elevation angle (El) of satellite from receiver, Eq. (1) can be written as

$$M_s = \frac{1}{d}\left[\sqrt{\left(r_s + \frac{d}{2}\right)^2 - \left(r_s \frac{R_e}{R_e + H}\cos El\right)^2} - \sqrt{\left(r_s - \frac{d}{2}\right)^2 - \left(r_s \frac{R_e}{R_e + H}\cos El\right)^2}\right] \tag{2}$$

where R_e is the radius of earth, and H is the shell height which is taken as hmF2.

Through a series expansion of Eq. (2) and taking a limit as the shell thickness d approaches to zero [30], the thick shell mapping function gets converted into a thin shell mapping function, M_t, given

as:

$$M_t = \frac{1}{\sqrt{1 - \left(\frac{R_e}{R_e + H}\cos El\right)^2}} \tag{3}$$

The estimation of shell height H and shell thickness d is discussed below.

2.1. Estimation of Shell Height and Thickness from IRI 2016 Data

For the estimation of shell height and thickness, the height of maximum electron density (hmF2), maximum electron density (NmF2) and VTEC were taken from (International Reference Ionosphere) IRI 2016, at 0400 and 1400 hours, on a monthly basis for the year 2018 at the latitude and longitude of Dehradun. The geographic (magnetic) latitude and longitude of Dehradun are 30.26°N (21.7154°N) and 77.99°E (152.9749°E), respectively. This location is outside the equatorial ionospheric anomaly region ($+/-15°$ magnetic latitude). The year 2018 falls at the end of solar cycle number 24 and is characterized by low solar activity. The maximum sunspot number (SSN) observed in January was 14.2, and it continuously decreased to 5.5 in December. Due to the variation in sun spot number, over the year, the height of maximum electron density and maximum electron density vary diurnally and seasonally. The average value of hmF2 was estimated as 267 km at 1400 hrs and 304 km at 0400 hrs. The shell thickness was estimated as 268 km and 242 km at 1400 hrs and 0400 hrs, respectively, as mentioned in Table 1. In the present analysis, the shell height and thickness are taken as 300 km and 250 km, respectively. This shell thickness of 250 km also matches the shell thickness predicted from GPS-TEC data collected in Delhi (28.58°N, 77.21°E) [36] which is latitude and longitude wise near Dehradun. However, the shell height of thin shell model, used in the present analysis, for comparison with thick shell model, is taken as 350 km since most of the investigations pursued in India are based on thin shell height of 350 km.

Table 1. Estimation of shell height and thickness using IRI 2016 data.

Time		04:00 hrs				14:00 hrs			
Month/Year	SSN	NmF2 (m^{-3})	hm2 (km)	VTEC (TECU)	Shell Thickness (km)	NmF2 (m^{-3})	hmF2 (km)	VTEC (TECU)	Shell thickness (km)
Nov.-17	15.4	5.80E+10	350	1.4	241	7.52E+11	250	19.4	257
Dec.-17	15	7.30E+10	300	1.8	245	5.62E+11	250	14.6	253
Jan.-18	14.2	7.80E+10	300	1.9	243	5.50E+11	250	14.2	253
Feb.-18	12.6	7.30E+10	300	1.8	245	7.60E+11	250	19.7	253
Mar.-18	9.9	6.50E+10	300	1.6	245	9.60E+11	250	25.8	268
Apr.-18	7.8	7.60E+10	300	1.9	250	1.17E+12	300	31.9	272
May-18	7.5	1.30E+11	300	3.4	261	9.90E+11	300	27.3	275
Jun.-18	7.2	1.25E+11	300	3	240	6.65E+11	300	19	285
Jul.-18	7	1.19E+11	300	2.9	243	5.40E+11	300	15.8	292
Aug.-18	6.7	8.50E+10	300	2	235	6.20E+11	250	18.1	291
Sep.-18	6.6	6.88E+10	300	1.6	234	8.14E+11	250	21.4	262
Oct.-18	6.9	6.59E+10	300	1.5	227	1.02E+12	250	25.8	252
		Average 304		Average 242		Average 267		Average 268	

3. DATA COLLECTION AND ANALYSIS

The IRNSS/GPS/SBAS (IGS) receiver and antenna were installed at Graphic Era University, Dehradun (30.26°N and 77.99°E) for data collection. The NavIC satellites data at dual frequencies S1 and L5 were

logged at every second with time stamping. The data from PRN 1 could not be recorded due to the unhealthy condition of the satellite. The number of days considered for data analysis in each month is given in Table 2. The minimum number of days is 11 in September and October 2018, and the maximum number of days is 27 in May 2018. In remaining all other months the number of days considered is more than 15. The reason for abrupt variation in number of days was unavailability of signal at any one or both the frequencies of transmission. The monthly data are divided into three categories, viz. winter (November, December, January, and February), equinoctial (March, April, September, and October)) and summer (May, June, July, and August) [36, 37].

Table 2. Availability of data during the period from November 2017 to October 2018.

Seasons	Winter				Summer				Equinoctial			
Year	2017		2018		2018				2018			
Month	11	12	01	02	05	06	07	08	03	04	09	10
No. of Days	18	20	25	20	27	21	17	16	20	23	11	11

The data (code and carrier phase measurement) collected at each epoch for all the satellites were analyzed for the determination of slant total electron content (STEC). The STEC values were converted into vertical total electron content (VTEC) at IPP using thick and thin shell mapping functions as discussed below. The vertical delay at S and L band frequencies was computed from the estimated VTEC values.

3.1. Estimation of Mapping Function

The values of mapping functions, as estimated from Eqs. (2) and (3), for the thick shell (M_s) and thin shell (M_t) models for different elevation angles are plotted in Fig. 2. The figure clearly shows that for elevation angles less than 30°, the value of the mapping function for the thick shell is higher than that for thin shell. It means that at lower elevation angles, the value of VTEC, at IPP, as estimated from STEC, will be lower for thick shell model than that for thin shell model. This finding is important for the position measuring navigation systems especially those using NavIC satellite system since NavIC satellites observe low elevation angle for most of the time of the day from the earth stations located in the northern part of India. Sample time series analyses of elevation angles of the NavIC geostationary satellites with PRN 3, 6, 7, and geosynchronous satellites with PRN 2, 4, 5, on June 14, 2018, are

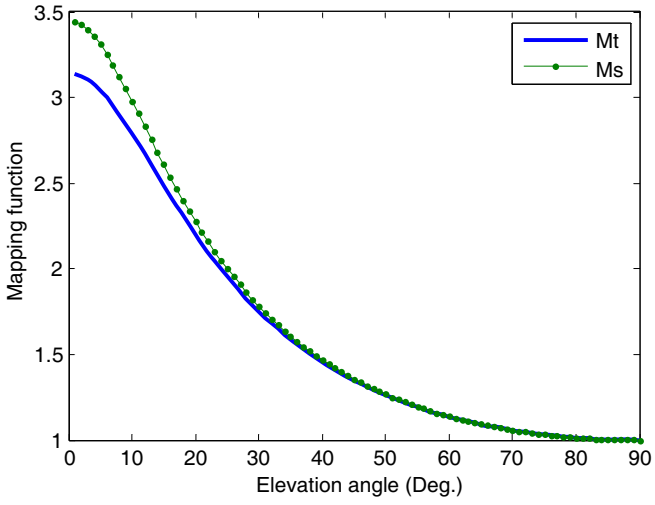

Figure 2. Comparison of thin and thick shell mapping functions.

plotted in Figs. 3(a) and (b), respectively. It can be seen that for geostationary satellites with PRN 6 and 7, the elevation angle is less than 30° for most of the day. For the satellite with PRN 3, the elevation angle is more than 50° for the whole day. In the case of geosynchronous satellites, the elevation angle is less than 30° for PRN 2 during night time, for PRN 4 during 1800 hrs to 0000 hrs, and PRN 5 during 0300 hrs to 1100 hrs.

The corresponding time series analyses of mapping functions for thick shell and thin-shell models are plotted in Figs. 3(c) and (d) for geostationary and geosynchronous satellites, respectively for June 14, 2018. In Fig. 3(c), a considerable difference in the value of mapping function, for the thick and thin shell model, can be seen for PRN 7 as this satellite observes low elevation angle (less than 30°) for all the times as shown in Fig. 3(a). In the case of PRN 3, the mapping functions overlap each other as this satellite observes a high elevation angle (more than 50°). A similar behavior of the mapping functions can be observed in Fig. 3(d) for geosynchronous satellites where for PRN 2, 4, and 5, the differences in mapping function values, during low elevation angle periods, are 0.087, 0.14, and 0.134, respectively. It can also be seen that during higher elevation angle time, the mapping functions are identical. These differences in mapping functions at the time of low elevation angles can introduce significant variations in the estimation of VTEC.

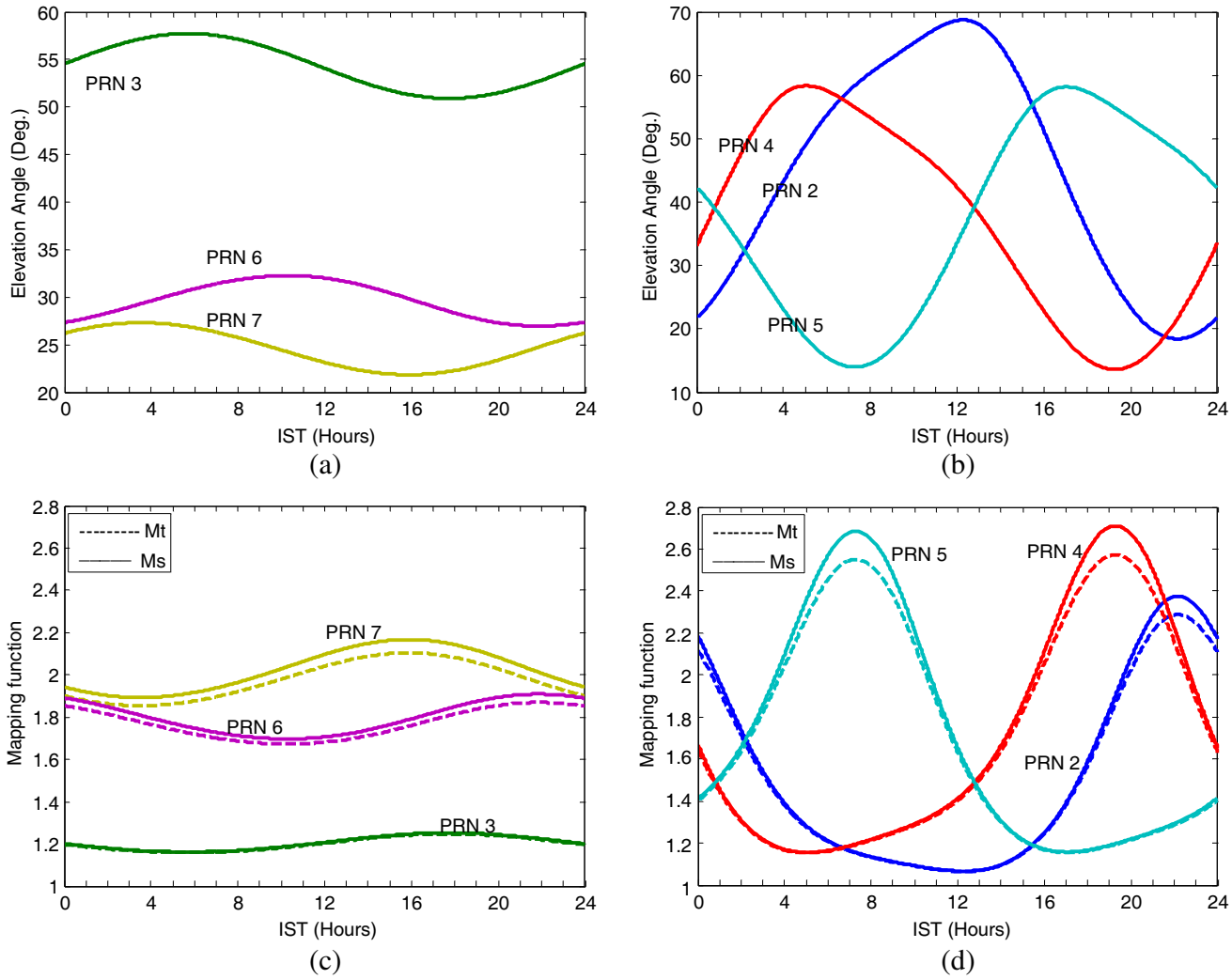

Figure 3. Time series analysis of elevation angel (a) geostationary satellites, (b) geosynchronous satellites, and mapping functions for thick and thin shell model, (c) geostationary satellites, (d) geosynchronous satellites of NavIC satellites (PRN 2-7), June 14, 2018.

3.2. Estimation of STEC and VTEC

The STEC was determined from the dual frequency code and carrier phase measurements. STEC from code measurements is given as [32]

$$\mathrm{STEC}_{\pounds} = \frac{1}{40.3}\left(\frac{f_1^2 f_2^2}{(f_1^2 - f_2^2)}\right)(\pounds_2 - \pounds_1) \tag{4}$$

where $\pounds_1$, $\pounds_2$ are measured code ranges in meter, and f_1, f_2 are frequencies of the signals transmitted from satellites.

For NavIC system, $f_1(S1) = 2492.08\,\mathrm{MHz}$ and $f_2(L5) = 1176.45\,\mathrm{MHz}$. At these frequencies, Eq. (4) is reduced to [33]:

$$\mathrm{STEC}_{\pounds} = 4.4192 \times 10^{16} \times (\pounds_2 - \pounds_1)\ [\mathrm{electron/m^2}] \tag{5}$$

or

$$\mathrm{STEC}_{\pounds} = 4.4192 \times (\pounds_2 - \pounds_1)\ [\mathrm{TECU}] \tag{6}$$

where one TEC unit (TECU) is 10^{16} electron/m^2.

Similarly, the STEC derived from carrier phase measurement can be written as:

$$\mathrm{STEC}_{\varphi} = 4.4192 \times (\varphi_1 - \varphi_2)\ [\mathrm{TECU}] \tag{7}$$

where φ_1 and φ_2 are the carrier phase ranges in meter.

The absolute STEC was derived by smoothing $\mathrm{STEC}_{\pounds}$ with STEC_{φ} [28, 32]. Furthermore, this smoothened STEC is still biased with satellite and receiver differential biases (DIBs). These biases arise due to the difference in path delay of signals at two frequencies (i.e., S1 and L5) within the satellite and receiver hardware. A five-state Kalman filter technique was used to estimate satellite and receiver DIBs [38]. The running of the Kalman filter requires initial satellite and receiver DIBs. The initial satellite DIBs were provided by Space Applications Centre (SAC), Indian Space Research Organization (ISRO), Govt. of India, Ahmedabad, and the initial receiver bias was estimated using Fitted Receiver Bias (FRB) technique [39]. Thus true STEC, herein after called STEC, was determined, after removal of the biases, at each epoch for the entire period of measurement, i.e., from November 2017 to October 2018 for all the satellites.

The temporal variability of the STEC as estimated for June 14, 2018, for all the satellites, is plotted in Fig. 4. The value of STEC at a particular time depends on the solar activity at that time, and the elevation angle of the satellite which determines the satellite-receiver slant path length through the ionosphere. The lower the elevation angle is, the larger the path length is, and hence, the larger the STEC will be at a particular time. As the maximum ionization takes place during the time interval

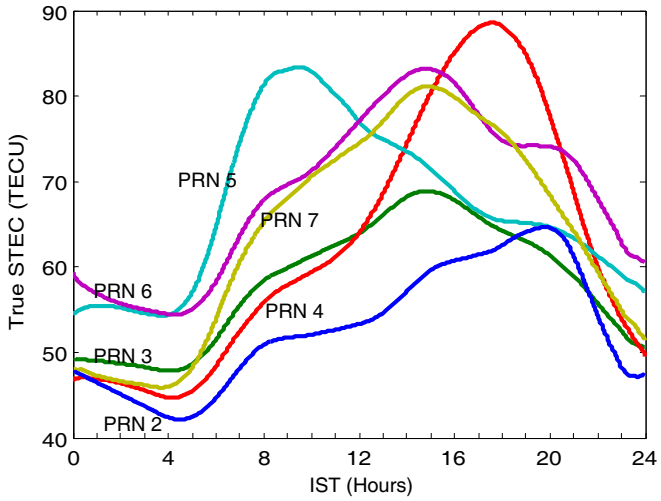

Figure 4. Diurnal variation of true STEC, June 14, 2018.

14:00 to 16:00 hrs, the peak of STEC for GEO satellites (PRN 3, 6, 7) can be observed at the same time duration in Fig. 4. The higher peak values of STEC for PRN 6 and 7, with respect to PRN 3, are mainly due to the low elevation angle for PRN 6 and 7 (Fig. 3(a)). In the cases of GSO satellites (PRN 2, 4, 5), the peaks of STECs are observed at different times of the day and with different magnitudes due to the large variation in elevation angle and hence in the slant path length.

The STEC values, as determined above, were converted into VTEC using the following relation:

$$\text{VTEC} = \frac{\text{STEC}}{M} \tag{8}$$

where M is the mapping function determined at IPP.

The VTEC values were determined for the entire period of measurement using mapping functions for thick and thin shell models. For illustration, the VTEC values thus estimated, using thick and thin shell mapping functions for June 14, 2018, for all the PRNs, are shown in Fig. 5. In the figure, the solid curves are for thick shell mapping function (M_s), and the dotted curves are for thin shell mapping function (M_t). The difference in VTECs estimated from the two mapping functions can be observed in cases of all the PRNs except for the satellite with PRN 3 where the difference is not significant due to high elevation angle of the satellite. By viewing Figs. 3 (elevation angle of the satellites) and 5 together, it can be seen that the maximum difference between the VTEC values estimated for thick and thin shell models occurs at the times when elevation angles of the satellites are the lowest, i.e., for PRN 2 during 22:00 hrs, PRN 4 during 19:00 hrs, PRN 5 during 7:00 hrs, and for PRN 6 and 7 during 16:00 hrs. These observations indicate the impact of ionospheric shell models on VTEC estimation when the elevation angle is low.

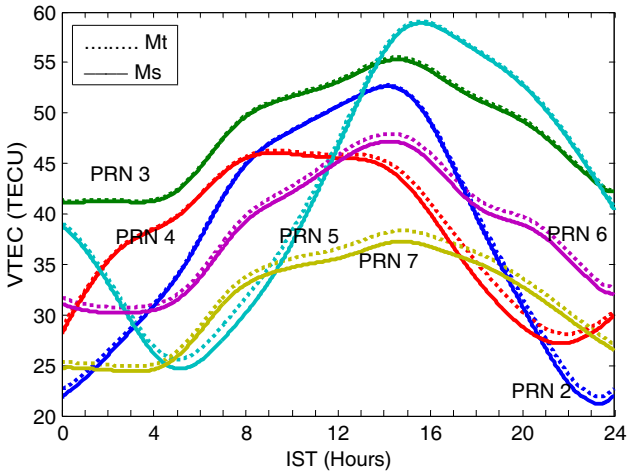

Figure 5. Diurnal variation of VTECs, estimated using thick and Thin shell models, June 14, 2018.

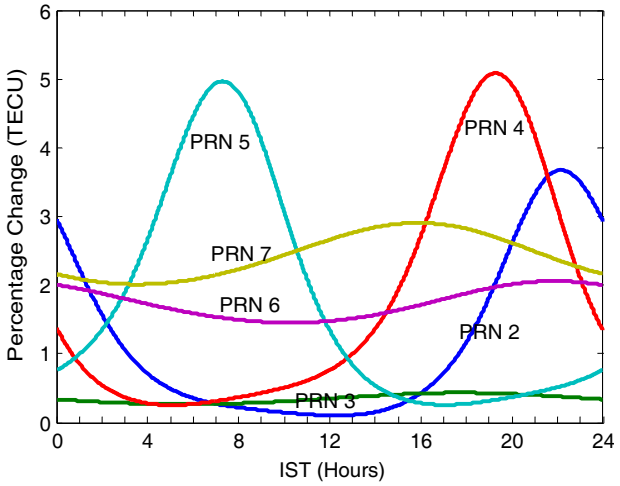

Figure 6. Diurnal variation of change in VTEC (%) using thick shell model with respect to thin shell model, June 14, 2018.

The diurnal variation of percentage change in estimated VTEC value from the two models is shown in Fig. 6. In the cases of PRN 4 and 5, the maximum change of around 5% is noted, on June 14, 2018. The vertical delay, which is determined by VTEC, can introduce a positional error up to 30 meters in satellite based navigation. Furthermore, the error in VTEC estimation due to the mapping function for low elevation angle satellites (Fig. 6) can introduce additional delay.

The vertical delay estimated from VTEC, at S1 and L5 frequencies, is discussed in the following section.

3.3. Ionospheric Vertical Delay

Vertical delay (I), at a frequency f, can be determined as [40]:

$$I = 40.3\frac{\text{VTEC}}{f^2} \text{ meters} \tag{9}$$

From Eq. (9) it is clear that at a particular frequency the vertical delay is a function of the VTEC value. As the estimated value VTEC using the thick shell model is less than that estimated using the thin shell model (Fig. 5), the corresponding maximum vertical delay differences ($I_t - I_s$) at S1 and L5 frequencies are shown in Fig. 7. From the figure, it can be observed that the maximum differences of vertical delays are 48 cm for PRN 4 and 45 cm for PRN 5 at L5 frequency. By correlating this observation with the elevation angles of these satellites (Fig. 3(b)) it can be said that the thick-shell ionospheric model significantly improves the vertical delays at low elevation angles. For PRN 3, the minimum delay difference can be observed which shows the expected performance of the thick shell model at higher elevations (Fig. 3(a)). However, the vertical delay differences at S1 frequency are smaller than L5. This is due to the higher frequency of S1 than L5 which is reciprocal and squared in Eq. (9). Thus for a single frequency user, the S1 frequency could be useful to combat the low elevation effect with the thick shell ionospheric model. These reductions in vertical delays at lower elevations could be very useful as the satellite navigation is used for precise positioning studies such as geodetic, seismic, tectonic motions, where positional accuracy of the order of millimeter or centimeter is required. Thus the thick shell model can be a better choice for NavIC systems as the satellites suffer from the low elevation angle most of the time, especially in the northern region.

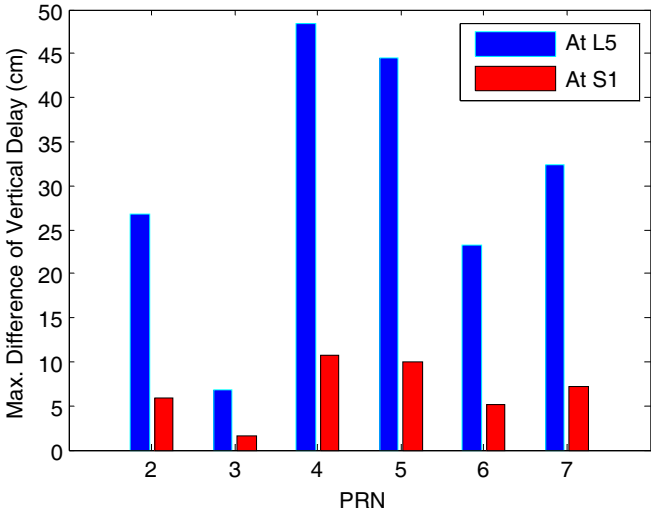

Figure 7. Maximum vertical delay difference using thin and thick shell at L5 and S1, June 14, 2018.

Further analysis of vertical delay at S1 and L5 frequencies using thick shell model has been carried out to assess its seasonal behavior. The vertical delay was computed, at each epoch for the period from November 2017 to October 2018 for PRN 2, 3, 4, 5, 6, and 7, using thick shell model. This duration was selected to cover all the three seasons of the year, i.e., winter (November, December, January, February), summer (May, June, July, August), and equinoctial (March, April, September, October). The vertical delay values at each epoch were converted into monthly mean values at each instant of the day (means the delay values at a particular instant of the day observed over the number of days of the month were averaged), and the same, with standard deviation, are plotted in Fig. 8 for S1 and L5 frequencies for all the PRNs and all the three seasons. The monthly curves have been grouped in three seasons because there was not much change in the monthly delay values over the season, but a significant variation was found in the seasonal analysis of the vertical delay. In Fig. 8, the upper curves are for vertical delay at L5 frequency, and the lower curves are for vertical delay at S1 frequency. A general observation of

the curves is that the maximum vertical delay has occurred during day time at around 1600 hrs and minimum during night and morning time at both the frequencies. Moreover, the maximum vertical delay values are more in summer and equinoctial months than winter months. At L5 frequency, the vertical delay varies from the maximum value of 18 m to a minimum value of 6 m irrespective of the month. The standard deviation of vertical delay at L5 is more in the daytime (1 to 4 m), near peak of the curve and lowest in the night time (0.1 to 0.5 m). In the case of equinoctial months, the standard deviation is more than that in other seasons. On the other hand, the vertical delay at S1 frequency does not show much temporal variability over the entire measurement period. The delay is slightly more during the daytime, and the mean delay over the day is around 2 m. The standard deviation in the case of S1 frequency is minimal (around 0.1 to 0.2 m).

The considerable temporal variability of vertical delay curves at L5 frequency, compared to that at S1 frequency, is due to the larger effect of VTEC temporal variability on vertical delay at L5 than S1 frequency, because of the frequency square term in Eq. (9). Due to the less variability of vertical delay at S1, there will be less uncertainty in the measurement of range between satellite and receiver. In a similar work [5], the ionospheric delay gradient has been estimated using S-band NavIC data over the low-latitude region to detect an equatorial plasma bubble (PBB) structure. This study shows a greater effect on the propagation of ionospheric radio waves and also suggests that the use of S-band NavIC signal can enhance the positional accuracy. Thus, compared to L5, S1 frequency is a better option for single-frequency NavIC users for ionospheric studies and navigational applications requiring higher positional accuracy in all the seasons and for all the satellites.

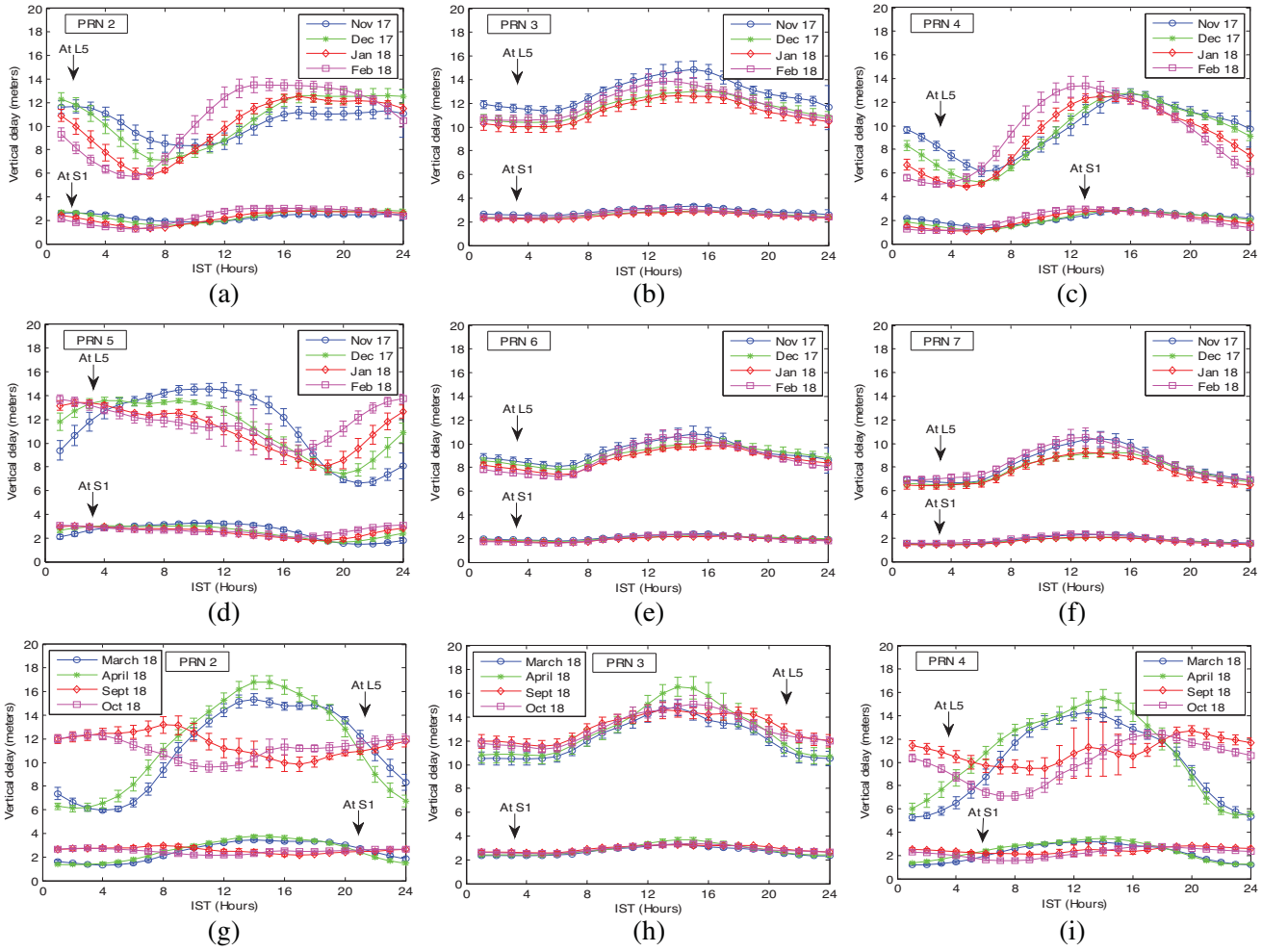

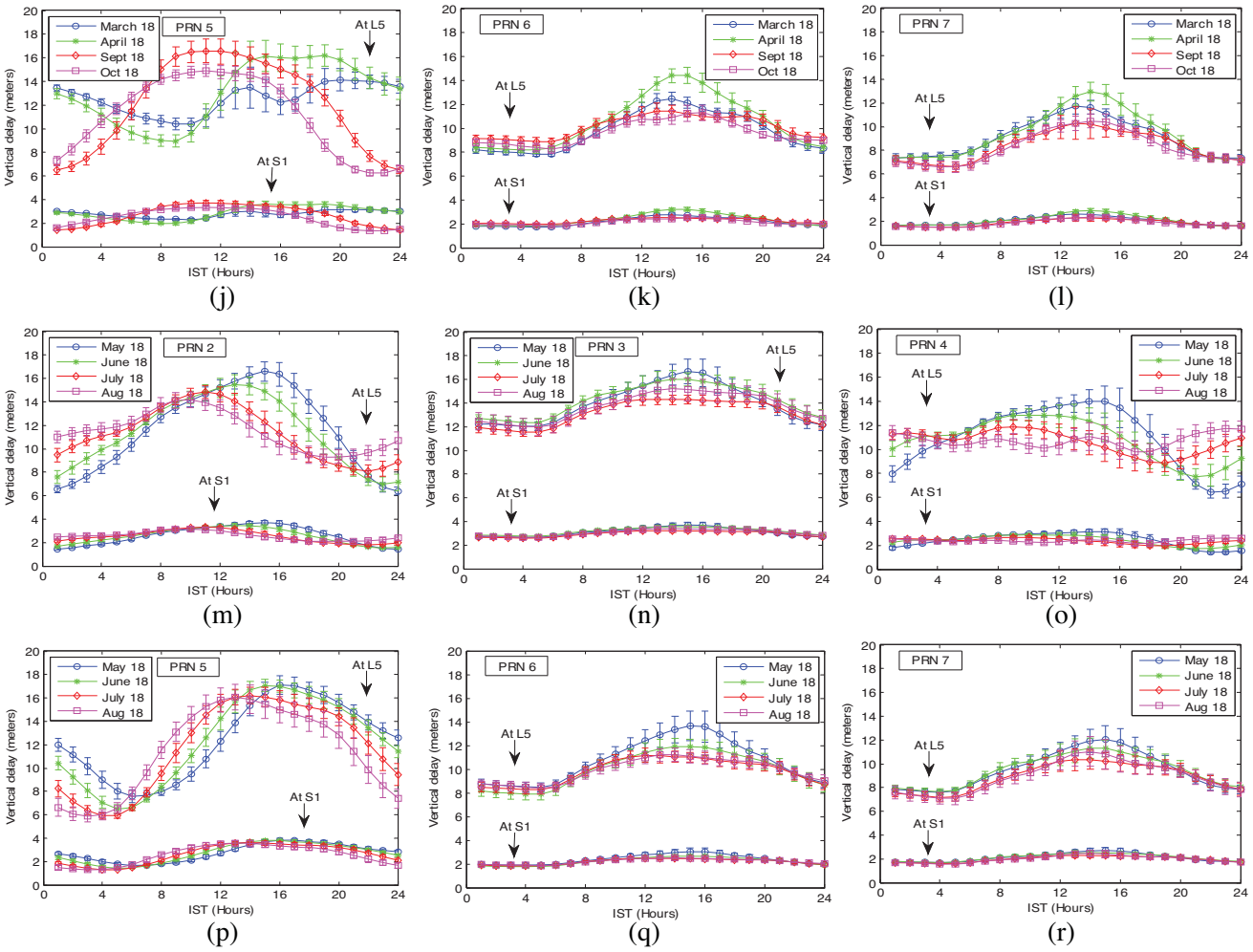

Figure 8. Diurnal variation of vertical delay at S1 and L5 based on thick shell model in winter months ((a) to (f)), equinoctial months ((g) to (l)), summer months ((m) to (r)) of 2017–18.

4. CONCLUSION

The ionospheric vertical delay can be determined directly by VTEC to improve the positional accuracy of the user. The estimation of VTEC is sensitive to the choice of ionospheric model (i.e., thick shell and thin shell) at low elevation angle as well as shell height, thus, based on ionospheric data taken from IRI2016, the height and thickness of the thick shell model were investigated and estimated as 300 km and 250 km, respectively. To find the suitability of the ionospheric model at low elevation, the mapping functions of thick shell and thin shell models have been compared. In comparison to the thin shell mapping function at low elevation angles, the thick shell mapping function has a higher value which results in a lower VTEC value and hence a reduction vertical delay. However, the two models have similar behaviors at high elevation angles. Thus the thick shell model is better suited for receivers having low elevation angles as in this case (Dehradun (30.26°N and 77.99°E)) and also in northern regions of India where low elevation of the NavIC satellites is observed (except PRN 3) for most of the time. Furthermore, a long term analysis has been carried out for ionospheric vertical delay, based on the thick shell ionospheric model using signals from the NavIC satellite system at S1 and L5 frequencies for the period from November 2017 to October 2018. The vertical delay at the S-band frequency was found to be less than that at the L-band frequency and is almost constant over a month.

The seasonal analysis of vertical delays shows considerable variation in vertical delay with time and

for all satellites at L5 frequency. On the other hand, the S1 frequency shows almost constant vertical delay for all seasons and all satellites, which reduces the complexity for the single frequency users. This finding encourages the use of the S1 frequency as this can be a better option than an L5 frequency to achieve better positional accuracy for single-frequency NavIC users. As the single frequency users need a vertical delay grid map to estimate the position with better accuracy, this study also gives the scope to determine a vertical delay grid map for the new NavIC satellite navigation system over the Indian region.

ACKNOWLEDGMENT

The authors would like to thank Space Applications Centre, Indian Space Research Organization (ISRO), Ahmadabad, India, for providing the necessary funds, receiving system and technical support for carrying out this research work under a sponsored research project.

REFERENCES

1. Rao, K. N. S., "GAGAN — The Indian satellite based augmentation system," *Indian Journal of Radio & Space Physics*, Vol. 36, 293–302, Aug. 2007.
2. Hager, B. H., R. W. King, and M. H. Murray, *Measurement of Crustal Deformation Using the Global Positioning System*, Vol. 19, 351, Annual Review of Earth and Planetary Sciences, 1991.
3. Sun, Y., R. Xue, D. Zhao, and D. Wang, "Radio frequency compatibility evaluation of S band navigation signals for future beidou," *Sensors (Switzerland)*, Vol. 17, No. 5, 1039, May 2017, doi: 10.3390/s17051039.
4. Zhong, J., J. Lei, X. Dou, and X. Yue, "Assessment of vertical TEC mapping functions for space-based GNSS observations," *GPS Solut.*, Vol. 20, No. 3, 353–362, Jul. 2016, doi: 10.1007/s10291-015-0444-6.
5. Ratnam, D. V., T. R. Vishnu, and P. B. S. Harsha, "Ionospheric gradients estimation and analysis of S-band navigation signals for NAVIC system," *IEEE Access*, Vol. 6, 66954–66962, 2018, doi: 10.1109/ACCESS.2018.2876795.
6. Schaer, S., "Mapping and predicting the earth's ionosphere using the Global Positioning System," *Diss. Astron. Inst.*, 205, 1999, [online], available: https://www.researchgate.net/publication/252260542_Mapping_and_Predicting_the_Earth's_Ionos-phere_Using_the_Global_Positioning_System.
7. Radicella, S. M., B. Nava, P. Coïsson, L. Kersley, and G. J. Bailey, "Effects of gradients of the electron density on Earth-space communications," *Ann. Geophys.*, Vol. 47, No. 2–3 suppl., 1227–1246, 2004, doi: 10.4401/ag-3296.
8. Bates, D. R., *The Propagation of Radio Waves*, Vol. 34, No. 6, K. G. Budden Cambridge University Press, Cambridge, 1985.
9. Abe, O. E., X. Otero Villamide, C. Paparini, S. M. Radicella, and B. Nava, "Analysis of a grid ionospheric vertical delay and its bounding errors over West African sub-Saharan region," *J. Atmos. Solar-Terrestrial Phys.*, Vol. 154, 67–74, Feb. 2017, doi: 10.1016/j.jastp.2016.12.015.
10. Hernández-Pajares, M., et al., "The ionosphere: Effects, GPS modeling and the benefits for space geodetic techniques," *J. Geod.*, Vol. 85, No. 12, 887–907, 2011, doi: 10.1007/s00190-011-0508-5.
11. Jiang, H., Z. Wang, J. An, J. Liu, N. Wang, and H. Li, "Influence of spatial gradients on ionospheric mapping using thin layer models," *GPS Solut.*, Vol. 22, No. 1, Jan. 2018, doi: 10.1007/s10291-017-0671-0.
12. Mannucci, A. J., B. D. Wilson, D. N. Yuan, C. H. Ho, U. J. Lindqwister, and T. F. Runge, "A global mapping technique for GPS-derived ionospheric total electron content measurements," *Radio Sci.*, Vol. 33, No. 3, 565–582, 1998, doi: 10.1029/97RS02707.
13. Klobuchar, J. A., "Ionospheric time-delay algorithm for single-frequency GPS users," *IEEE Trans. Aerosp. Electron. Syst.*, Vol. 23, No. 3, 325–331, 1987, doi: 10.1109/TAES.1987.310829.

14. Walter, T., et al., "Robust detection of ionospheric irregularities," *Navig. J. Inst. Navig.*, Vol. 48, No. 2, 89–100, 2001, doi: 10.1002/j.2161-4296.2001.tb00231.x.
15. Ruffini, G., A. Flores, and A. Rius, "GPS tomography of the ionospheric electron content with a correlation functional," *IEEE Trans. Geosci. Remote Sens.*, Vol. 36, No. 1, 143–153, 1998, doi: 10.1109/36.655324.
16. Wen, D., Y. Yuan, J. Ou, K. Zhang, and K. Liu, "A hybrid reconstruction algorithm for 3-D ionospheric tomography," *IEEE Trans. Geosci. Remote Sens.*, Vol. 46, No. 6, 1733–1739, 2008, doi: 10.1109/TGRS.2008.916466.
17. Shukla, A. K., M. R. Sivaraman, and K. Bandyopadhyay, "A comparison study of voxel based multi- and two-layer ionospheric tomography models over the indian region using GPS data," *Int. J. Remote Sens.*, Vol. 31, No. 10, 2535–2549, 2010, doi: 10.1080/01431160903019296.
18. Shukla, A. K., S. Das, N. Nagori, M. R. Sivaraman, and K. Bandyopadhyay, "Two-shell ionospheric model for Indian region: A novel approach," *IEEE Trans. Geosci. Remote Sens.*, Vol. 47, No. 8, 2407–2412, 2009, doi: 10.1109/TGRS.2009.2017520.
19. Komjathy, A., et al., "A new ionospheric model for wide area differential GPS?: The multiple shell approach," *Network*, 28–30, Jan. 2002.
20. Norsuzila, Y., M. Abdullah, and M. Ismail, "Determination of GPS total electron content using Single Layer Model (SLM) ionospheric mapping function," *IJCSNS Int. J. Comput. Sci. Netw. Secur.*, Vol. 8, No. 9, 154–160, 2008, [online], available: http://paper.ijcsns.org/07_book/200809/20080922.pdf.
21. Tancredi, U., A. Renga, and M. Grassi, "Geometric total electron content models for topside ionospheric sounding," *EESMS 2014 — 2014 IEEE Work. Environ. Energy Struct. Monit. Syst. Proc.*, 163–168, 2014, doi: 10.1109/EESMS.2014.6923285.
22. Niranjan, K., B. Srivani, S. Gopikrishna, and P. V. S. Rama Rao, "Spatial distribution of ionization in the equatorial and low-latitude ionosphere of the Indian sector and its effect on the pierce point altitude for GPS applications during low solar activity periods," *J. Geophys. Res. Sp. Phys.*, Vol. 112, No. 5, 1–15, 2007, doi: 10.1029/2006JA011989.
23. Xiang, Y. and Y. Gao, "An enhanced mapping function with ionospheric varying height," *Remote Sens.*, Vol. 11, No. 12, 1497, Jun. 2019, doi: 10.3390/rs11121497.
24. Lanyi, G. E. and T. Roth, "A comparison of mapped and measured total ionospheric electron content using global positioning system and beacon satellite observations," *Radio Sci.*, Vol. 23, No. 4, 483–492, 1988, doi: 10.1029/RS023i004p00483.
25. Hernàndez-Pajares, M., J. M. Juan, J. Sanz, and M. Garcia-Fernàndez, "Towards a more realistic ionospheric mapping function," *XXVIII URSI Gen. Assem.*, Vol. 2002, 2002–2005, 2005.
26. Brunini, C., E. Camilion, and F. Azpilicueta, "Simulation study of the influence of the ionospheric layer height in the thin layer ionospheric model," *J. Geod.*, Vol. 85, No. 9, 637–645, 2011, doi: 10.1007/s00190-011-0470-2.
27. Prasad, S. N. V. S., P. V. S. Rama Rao, D. S. V. V. D. Prasad, K. Venkatesh, and K. Niranjan, "On the variabilities of the Total Electron Content (TEC) over the Indian low latitude sector," *Adv. Sp. Res.*, Vol. 49, No. 5, 898–913, 2012, doi: 10.1016/j.asr.2011.12.020.
28. Acharya, R., et al., "Ionospheric studies for the implementation of GAGAN," *Indian J. Radio Sp. Phys.*, Vol. 36, No. 5, 394–404, 2007.
29. Ratnam, D. V., J. R. K. K. Dabbakuti, and S. Sunda, "Modeling of ionospheric time delays based on a multishell spherical harmonics function approach," *IEEE J. Sel. Top. Appl. Earth Obs. Remote Sens.*, Vol. 10, No. 12, 5784–5790, 2017, doi: 10.1109/JSTARS.2017.2743695.
30. Smith, D. A., E. A. Araujo-Pradere, C. Minter, and T. Fuller-Rowell, "A comprehensive evaluation of the errors inherent in the use of a two-dimensional shell for modeling the ionosphere," *Radio Sci.*, Vol. 43, No. 6, n/a-n/a, 2008, doi: 10.1029/2007rs003769.
31. Maruyama, T., K. Hozumi, and G. Ma, "Ionospheric total electron content derived from gnss signals by double thin-shell model near the magnetic equator and implication in the meridional wind," *2019 Russ. Open Conf. Radio Wave Propagation, RWP 2019 — Proc.*, Vol. 1, No. 3, 139–140, 2019, doi: 10.1109/RWP.2019.8810250.

32. Sinha, S., R. Mathur, S. C. Bharadwaj, A. Vidyarthi, B. S. Jassal, and A. K. Shukla, "Estimation and smoothing of tec from navic dual frequency data," *2018 4th Int. Conf. Comput. Commun. Autom. ICCCA 2018*, 1–5, 2018, doi: 10.1109/CCAA.2018.8777665.
33. Bhardwaj, S. C., A. Vidyarthi, B. S. Jassal, and A. K. Shukla, "Study of temporal variation of vertical TEC using NavIC data," *2017 International Conference on Emerging Trends in Computing and Communication Technologies, ICETCCT 2017*, Vol. 2018-Janua, 1–5, 2018, doi: 10.1109/ICETCCT.2017.8280317.
34. Zaminpardaz, S., P. J. G. Teunissen, and N. Nadarajah, "IRNSS stand-alone positioning: First results in Australia," *J. Spat. Sci.*, Vol. 61, No. 1, 5–27, 2016, doi: 10.1080/14498596.2016.1142398.
35. Bilitza, D., et al., "International reference ionosphere 2016: From ionospheric climate to real-time weather predictions," *Sp. Weather*, Vol. 15, No. 2, 418–429, 2017, doi: 10.1002/2016SW001593.
36. Venkatesh, K., P. V. S. R. Rao, D. S. V. V. D. Prasad, K. Niranjan, and P. L. Saranya, "Study of TEC, slab-thickness and neutral temperature of the thermosphere in the Indian low latitude sector," *Ann. Geophys.*, Vol. 29, No. 9, 1635–1645, 2011, doi: 10.5194/angeo-29-1635-2011.
37. Bagiya, M. S., H. P. Joshi, K. N. Iyer, M. Aggarwal, S. Ravindran, and B. M. Pathan, "TEC variations during low solar activity period (2005–2007) near the Equatorial Ionospheric Anomaly Crest region in India," *Ann. Geophys.*, Vol. 27, 1047–1057, 2009.
38. Bhardwaj, S. C., A. Vidyarthi, B. S. Jassal, and A. K. Shukla, "Estimation of temporal variability of differential instrumental biases of NavIC satellites and receiver using Kalman filter," *Radio Sci.*, Jun. 2020, doi: 10.1029/2019RS006886.
39. Sunehra, D., "TEC and instrumental bias estimation of GAGAN station using Kalman filter and SCORE algorithm," *Positioning*, Vol. 7, No. 1, 41–50, 2016, doi: 10.4236/pos.2016.71004.
40. Kashcheyev, A., B. Nava, and S. M. Radicella, "Estimation of higher-order ionospheric errors in GNSS positioning using a realistic 3-D electron density model," *Radio Sci.*, Vol. 47, No. 4, 1–7, 2012, doi: 10.1029/2011RS004976.